JB
Journals.ASM.org

Cytochrome cd_1 Nitrite Reductase NirS Is Involved in Anaerobic Magnetite Biomineralization in *Magnetospirillum gryphiswaldense* and Requires NirN for Proper d_1 Heme Assembly

Yingjie Li,[a] Shilpa Bali,[b] Sarah Borg,[a] Emanuel Katzmann,[a] Stuart J. Ferguson,[b] Dirk Schüler[a]

Ludwig-Maximilians-Universität München, Department Biologie I, Mikrobiologie, Planegg-Martinsried, Germany[a]; Department of Biochemistry, University of Oxford, Oxford, United Kingdom[b]

The alphaproteobacterium *Magnetospirillum gryphiswaldense* synthesizes magnetosomes, which are membrane-enveloped crystals of magnetite. Here we show that nitrite reduction is involved in redox control during anaerobic biomineralization of the mixed-valence iron oxide magnetite. The cytochrome cd_1-type nitrite reductase NirS shares conspicuous sequence similarity with NirN, which is also encoded within a larger *nir* cluster. Deletion of any one of these two *nir* genes resulted in impaired growth and smaller, fewer, and aberrantly shaped magnetite crystals during nitrate reduction. However, whereas nitrite reduction was completely abolished in the Δ*nirS* mutant, attenuated but significant nitrite reduction occurred in the Δ*nirN* mutant, indicating that only NirS is a nitrite reductase in *M. gryphiswaldense*. However, the Δ*nirN* mutant produced a different form of periplasmic d_1 heme that was not noncovalently bound to NirS, indicating that NirN is required for full reductase activity by maintaining a proper form of d_1 heme for *holo*-cytochrome cd_1 assembly. In conclusion, we assign for the first time a physiological function to NirN and demonstrate that effective nitrite reduction is required for biomineralization of wild-type crystals, probably by contributing to oxidation of ferrous iron under oxygen-limited conditions.

Magnetosomes are bacterial organelles used by magnetotactic bacteria (MTB) for orientation in the Earth's magnetic field to search for growth-favoring suboxic zones of stratified aquatic sediments (1). In the freshwater alphaproteobacterium *Magnetospirillum gryphiswaldense* MSR-1 (here referred to as MSR-1) and related MTB, the magnetosomes are membrane-enveloped crystals of magnetite (Fe_3O_4) (1). Magnetosome synthesis and assembly is controlled by a number of specific proteins, which are mostly encoded within a genomic magnetosome island (2–4). It has been proposed that biomineralization of the mixed-valence iron oxide magnetite (Fe_3O_4) takes place within the magnetosomal membrane vesicles by coprecipitation of ferrous and ferric iron, via supersaturating concentrations, which are favored by a low redox potential (5–7). Magnetite synthesis occurs only under suboxic conditions (8, 9), and previous observations indicated that magnetosome synthesis might be linked to denitrification (10, 11). Bacterial denitrification is a respiratory process in which nitrate is stepwise reduced to nitrogen gas ($NO_3^- \rightarrow NO_2^- \rightarrow NO \rightarrow N_2O \rightarrow N_2$) (12). Recently, we showed that MSR-1 is capable of anaerobic growth by a complete pathway of denitrification, including gene functions for nitrate (*nap*), nitrite (*nirS*), nitric oxide (*nor*), and nitrous oxide reduction (*nos*) (13). Except for *nap*, which was upregulated by oxygen, the highest expression of other denitrification genes coincided with conditions permitting maximum magnetite synthesis (low oxygen tensions and the presence of nitrate), whereas microaerobic denitrification overlapped with oxygen respiration (13). The deletion of *nap* genes encoding a periplasmic nitrate reductase, but not *nor* or *nos*, abolished anaerobic growth and also delayed aerobic growth in both nitrate and ammonium medium. Inactivation of *nap* also severely impaired magnetite biomineralization and resulted in fewer, smaller, and irregular crystals during denitrification and also microaerobic respiration, demonstrating that the periplasmic nitrate reductase Nap is involved in redox control of magnetite biomineralization (13).

Earlier work suggested that also the second step of denitrification, the reduction of nitrite to nitric oxide ($NO_2^- \rightarrow NO$), might be involved in magnetite biomineralization in magnetospirilla. This was based on the observation that the cytochrome cd_1-type nitrite reductase NirS purified from *Magnetospirillum magnetoticum* accelerated the oxidization of ferrous iron in the presence of nitrite under anaerobic conditions *in vitro* (14), indicating that this enzyme possesses a novel Fe(II):nitrite oxidoreductase activity that may participate in magnetosomal Fe_3O_4 synthesis *in vivo*. However, due to the lack of genetic evidence, the exact functions of NirS in denitrifying growth and magnetite biomineralization have remained unexplored. NirS, the cytochrome cd_1-type nitrite reductase, occurs in many denitrifying bacteria, while in others, reduction of nitrite to nitric oxide can also be catalyzed by another type of enzyme, the trimeric copper-containing protein NirK (12). NirS functions as periplasmic homodimeric hemoprotein, in which each subunit contains a covalent *c*-type and a unique noncovalent d_1-type heme. NirS is the only protein known to contain the d_1 heme as an essential cofactor, which is assumed to be the catalytic site for nitrite reduction (15). Heme d_1 biogenesis is

Received 11 June 2013 Accepted 18 July 2013
Published ahead of print 26 July 2013
Address correspondence to Stuart J. Ferguson, stuart.ferguson@bioch.ox.ac.uk, or Dirk Schüler, dirk.schueler@lrz.uni-muenchen.de.
Supplemental material for this article may be found at http://dx.doi.org/10.1128/JB.00686-13.

doi:10.1128/JB.00686-13

thought to be mediated by a set of further proteins encoded within the *nir* operon (16–18).

Here, we set out to investigate the role of NirS in nitrite reduction and in magnetite biosynthesis in the magnetic bacterium MSR-1. The conspicuous high sequence similarity of NirS to one (NirN) of the proteins encoded in the identified *nir* gene cluster prompted us to investigate the functions of both of these proteins in denitrifying growth as well as magnetite biosynthesis. Genetic and biochemical analyses revealed that only NirS is a nitrite reductase, but NirN is required for its full activity by either maintaining a correct form of d_1 heme for NirS or by acting during assembly of d_1 heme in *holo*-cytochrome cd_1 nitrite reductase; this for the first time assigns a physiological function to NirN. Moreover, deletions of *nirS* and *nirN* also impaired magnetite biomineralization, and functional NirS participates in redox control, probably by contributing to oxidation of ferrous iron under oxygen-limited conditions.

MATERIALS AND METHODS

Bacterial strains and growth conditions. Bacteria strains and plasmids used in this work are shown in Tables S1 and S2 in the supplemental material. *Escherichia coli* strains were cultured in lysogeny broth (LB) broth at 37°C. MSR-1 strains were grown at 30°C in nitrate medium if not specified otherwise (13). Nitrate was replaced with 4 mM ammonium chloride in the ammonium medium. In low-iron medium (LIM), ferric citrate was omitted from the nitrate medium (19). When necessary, antibiotics were added at the following concentration: for *E. coli*, tetracycline (Tc) at 12 μg/ml, kanamycin (Km) at 25 μg/ml; for MSR-1, Tc at 5 μg/ml, Km at 5 μg/ml. Diaminopimelic acid (DAP) at 300 μM was added to the medium when *E. coli* strain BW29427 was used as the donor for conjugation.

Experiments for growth and measurement of the magnetic response (C_{mag}, the ratio of scattering intensities at different angles of the magnetic field relative to the light beam [20]) were carried out under microaerobic and anaerobic conditions in 250-ml flasks containing 100 ml medium. For microaerobic conditions, prior to autoclaving, flasks were sealed with butyl rubber stoppers under a microoxic gas mixture containing 2% O_2 and 98% N_2. When oxygen was omitted from the gas mixture, anaerobic conditions were achieved. For aerobic conditions, cells were cultured in an environment with free gas exchange with air in 300-ml flasks containing 20 ml medium agitated at 200 rpm. The optical density (OD) and the magnetic response (C_{mag}) were monitored photometrically at 565 nm as previously described (21). For the gas production assay, cells were inoculated to a final OD_{565} of about 0.02 and mixed with nitrate medium with 0.3% agar in oxygen gradient tubes and exposed to air. If not specified, inocula were prepared aerobically by repeated passaging in fresh nitrate medium to a final C_{mag} value of 0.

Genetic and molecular biology techniques. Standard molecular and genetic techniques were performed for DNA isolation, digestion, ligation, and transformation (22). All DNA products were sequenced using BigDye Terminator version 3.1 chemistry on an ABI 3700 capillary sequencer (Applied Biosystems, Darmstadt, Germany). Sequence data were analyzed with the software Vector NTI Advance 11.5.1 (Invitrogen, Darmstadt, Germany). All oligonucleotide sequences used in this study are available if required.

Identification of a *nir* cluster. Because *nir* genes were located on two different contigs of the incomplete genome assembly of MSR-1, a PCR amplicon, obtained with primers nirB-down-F and nirC-up-R, comprising the missing *nirE* gene was used to bridge the gap between a 6,541-bp contig (containing nucleotide sequence from 286116 to 292656) and a 50,562-bp contig (nucleotide sequence from 2411316 to 2461877). The nirE sequence was submitted to GenBank (see below).

Construction of mutant strains. All PCRs were performed by using Phusion polymerase (NEB). Enzymes in this work, including restriction enzymes and T4 DNA ligase, were purchased from Fermentas. A two-step, *cre-lox*-based method was used to generate unmarked deletions of *nirS* and *nirN*, respectively (13). The plasmid used to delete the *nirS* gene was constructed in two steps. First, a 2-kb downstream PCR fragment of *nirS* was digested with NdeI and KpnI and cloned into pCM184 to yield pLYJ06. Second, the 2-kb upstream PCR product of *nirS* was ligated into SacI/AgeI-digested pLYJ06 to yield *nirS* deletion plasmid pLYJ08. For *nirN* deletion, the 2-kb upstream PCR product was cloned into pCM184 between Acc65I and NotI sites, generating pLYJ20. An approximately 2-kb downstream fragment of *nirN* was then ligated into MluI/SacI-digested pLYJ20 to obtain pLYJ23. After that, allelic exchange vectors pLYJ08 and pLYJ23 were transformed into MSR-1 by conjugation. First, deletion mutants were screened on replica plates with kanamycin and tetracycline. Then, screening PCR was performed for colonies that did not grow on tetracycline plates. To generate unmarked deletion mutants, pLYJ86 was constructed by ligating *cre* genes from pCM157 into SmaI/XbaI-digested pLYJ36. After that, the *nirS* promoter region and *cre* fusion from pLYJ86 was digested with Acc65I and XbaI and cloned into pBBR1MCS-3 to generate pLYJ87. The plasmid pLYJ87 was then transformed into each mutant and subsequently cured from each mutant by several transfers in nitrate medium without any antibiotics. Unmarked mutants were finally designated Δ*nirS* and Δ*nirN* mutants, respectively.

Complementation experiments. For genetic complementation of the Δ*nirS* and Δ*nirN* mutants, two plasmids based on pBBR1MCS-2 were generated. For complementation of *nirS*, pLYJ51 was used, in which the *nirS* gene sequence with its own promoter region was ligated into Acc65I-digested pBBR1MCS-2. Other *nirS* genes from *Magnetospirillum magneticum* (*amb1395* and *amb4165*) and *Pseudomonas stutzeri* (*PST_3532*) were also hetero-complemented into the Δ*nirS* strain. The *nirS* promoter region from MSR-1 was ligated into Acc65I/HindIII-digested pBBR1MCS-2 to generate pLYJ36. Subsequently, *amb1395* and *amb4165* were cloned into HindIII/SmaI-digested pLYJ36 to obtain pLYJ88 and pLYJ89, respectively. The PCR fragment of *PST_3532* was digested with HindIII and XbaI and ligated into pLYJ36 to yield pLYJ95. The *nirN* gene sequence was digested with ApaI and SacI and cloned into pRU1 to yield pLYJ74. *nirN* gene from *M. magneticum* (*amb1408*) was ligated into ApaI/SacI-digested pRU1 to obtain pLYJ113. *nirN* from *P. stutzeri* (*PST_3538*) was cloned into pLYJ36 between HindIII and XbaI sites, yielding pLYJ124.

Chemical analysis. For nitrate and nitrite analyses, MSR-1 cells were grown under anaerobic conditions at 20°C, at which nitrate and nitrite was reduced more slowly. The nitrate concentration was measured using Szechrome reagents (Polysciences, Inc.). Diluted 20-fold samples of cultures were prepared, and Szechrome reagents were subsequently added. The absorbance was recorded at 570 nm after 0.5 hour. When nitrate was no longer detectable, samples without dilution were used to confirm the absence of nitrate. A nitrate standard curve (0 to 350 μM) was generated to convert absorbance values to concentrations.

Nitrite was detected by using the modified Griess reagent (Sigma). Samples of 100 μl of cultures diluted 20-fold were reacted with an equal amount of modified Griess reagent, and after 15 min the absorbance at 540 nm was recorded. When no nitrite was found, cultures without dilution were used to confirm the absence of nitrite. A nitrite standard curve (0 to 70 μM) was obtained to calculate the final nitrite concentration.

Preparation of the periplasmic fraction and purification of cytochrome cd_1. For the preparation of the periplasmic fraction and NirS purification, large quantities (100 liters for each strain) of anaerobic cultivated cells were obtained at 20°C in a fermentor (Sartorius, Göttingen, Germany), in which 1 g/liter peptone was added while HEPES and a trace element mixture were omitted from the nitrate medium. The pH of the culture was maintained by the addition of either H_2SO_4 (1 M) or NaOH (1 M) via peristaltic pumps. After harvesting at 4°C, 3-g (wet weight) cell pellets were resuspended in 15 ml of SET buffer (0.5 M sucrose, 200 mM Tris-HCl [pH 7.5], 1 mM EDTA). Culture with lysozyme (15 mg/liter) was added, immediately followed by 15 ml of ice-cold water to administer a mild osmotic shock. This mixture was incubated at 37°C for 30 min and

then centrifuged at 9,000 × *g* for 15 min. The supernatant was retained as the periplasmic fraction. Purification of cytochrome cd_1 was carried out as described in reference 14 with slight modifications. Briefly, purification was done at room temperature, and the periplasmic extracts were diluted 4 times before loading onto a DEAE-Sepharose column equilibrated with 50 mM Tris-HCl (pH 8.0). NirS in the flowthrough was dialyzed against 10 mM sodium phosphate (pH 6.5) for 12 h, and the desalted solution was further applied to a carboxymethyl (CM)-Toyopearl column. NirS was eluted with a linear gradient of 0 to 0.5 M NaCl. For the cytochrome cd_1 (NirS) fraction, solid ammonium sulfate was added to 40% saturation. After slow stirring for 1 h at 4°C, the solution was centrifuged at 10,000 × *g* for 20 min. Solid ammonium sulfate was further added to the supernatant up to 80% saturation. The suspension was again stirred for 1 h at 4°C and centrifuged at 8,000 × *g* for 20 min. The supernatant was applied to a CM-32 column equilibrated with 10 mM sodium phosphate, pH 6.5, containing 80% saturated ammonium sulfate solution. The cytochrome cd_1, adsorbed on the column, was washed with the same buffer used for equilibration. The enzyme was subsequently eluted with 10 mM sodium phosphate, pH 6.5, containing 0.2 M NaCl, and buffer was exchanged into 50 mM Tris-HCl, pH 7.5.

Heme staining. Activity staining of SDS-polyacrylamide gels for the covalently bound heme was conducted using the method described in reference 23. Briefly, the gel was soaked in 70 ml of 0.5 M sodium acetate (pH 5.0) for 20 min, followed by addition of 30 ml methanol containing 3 mg of *N*,*N*,*N*′,*N*′-tetramethylbenzidine (TMBZ). After shaking the gel for 5 min, 100 μl of H_2O_2 was added to develop the bands for detection of hemoproteins.

Absorbance spectra detection. UV-visible spectra were acquired on a PerkinElmer 3 UV-visible scanning spectrophotometer at room temperature, using fused quartz cuvettes with a 1-cm path length (Merck) and samples that were in 50 mM Tris-HCl buffer at pH 7.5. Pyridine hemochrome spectra were obtained according to the method of Bartsch (24) using 5 μM protein in 19% (vol/vol) pyridine and 0.15 M NaOH.

Analysis of transcriptional *gusA* fusions. To generate the transcriptional *nirTBECFDLGHJN-gusA* fusion plasmids, the *nirTBECFDLGHJN* promoter region was cloned into Acc65I/HindIII-digested pLYJ97, designated pLYJ104. To investigate the expression of *nirS* under different conditions, pLYJ94 containing the *nirS* promoter fused with *gusA* was used. Then pLYJ104 and pLYJ94 were introduced into MSR-1 wild-type (WT) and Δ*nirS* strains, respectively, by conjugation. β-Glucuronidase activity was determined at 37°C as described before (13). Units were recorded as nanomoles of product formed per minute. Triplicate assays were conducted, and the values reported are averages from at least two independent experiments.

Growth experiments with different iron sources. To determine effects of different iron sources on MSR-1 WT and Δ*nirS* strains, exponential-phase iron-deprived nonmagnetic precultures (200 ml) of MSR-1 WT and Δ*nirS* strains were obtained by culturing cells in LIM under microaerobic conditions. Concentrated cells were washed twice by using nitrate-free LIM and subsequently suspended in LIM in the presence (LIM) or absence (nitrate-free LIM) of nitrate to a final OD_{565} of 0.1. Prior to inoculation, either an anoxic ferrous chloride or ferric chloride stock was added to a final concentration of 100 μM for the anaerobic growth medium. Reduced iron was maintained by adding 0.2 mM sodium ascorbate. A preliminary experiment has shown that 0.2 mM sodium ascorbate alone has no effect on growth and magnetite biomineralization (data not shown). As revealed by the ferrozine assay, all iron in the medium was in the ferrous form in the presence of ascorbate, whereas in the absence of the reductant all added iron remained in the ferric form. Then, iron-deprived nonmagnetic cells were inoculated to a final OD_{565} of 0.1. After a 6-hour iron induction, the C_{mag} was measured, and extracellular iron concentrations were quantified at 562 nm in a ferrozine assay (25). For the analysis of Fe(II), 100 μl of sample was added into 900 μl 1 M HCl in an anaerobic chamber and determined directly by a ferrozine assay. Total iron [Fe(II) and Fe(III)] was measured by reducing 100 μl of sample with hydroxylamine hydrochloride before addition of the ferrozine reagent. The amount of Fe(III) was calculated by subtracting the amount of Fe(II) from the total Fe.

Construction of the NirS-mCherry fusion protein and fluorescence microscopy. For construction of the NirS-mCherry fusion protein, first the *nirS* sequence without the putative promoter region or candidate signal peptides was amplified using a forward primer, that included a 12-amino-acid linker sequence at the 5′ end, and cloned between SmaI and XbaI sites of pBBR1MCS-2 to give plasmid pLYJ52. Subsequently, the putative *nirS* promoter region together with the candidate signal peptide was cloned into Acc65I/HindIII-digested pLYJ52 to obtain pLYJ59. To generate an N-terminal *mcherry* fusion, *mcherry* was amplified from pFM208 and inserted into HindIII/SmaI-digested pLYJ59 to generate plasmid pLYJ64. Then, MSR-1 WT and Δ*nirS* strains containing plasmid pLYJ64 were cultured in Hungate tubes under microaerobic conditions for 16 h and immobilized on agarose pads (flask standard medium salts in water, supplemented with 1% agarose) as described previously (26).

The localization of mCherry-tagged proteins was then determined using an Olympus IX81 fluorescence microscope equipped with a Hamamatsu Orca-ER camera. The excitation wavelength for mCherry was 587 nm and emission was recorded at 610 nm.

Transmission electron microscopy (TEM) and crystal analysis. If not specified, MSR-1 WT and mutants were grown at 25°C under anaerobic conditions for 24 h, concentrated, and adsorbed onto carbon-coated copper grids. Samples were viewed and recorded with a TECNAI F20 microscope (FEI, Eindhoven, Netherlands) at 200 kV or a Morgagni 268 microscope (FEI, Eindhoven, Netherlands) at 80 kV as previously described (27). For magnetosome analysis, more than 300 crystals and 100 cells were detected for each strain.

Bioinformatic analysis. Using respective protein sequences from *Pseudomonas aeruginosa* as a query in a BLASTP analysis, *nirS* and *nirN* genes were identified by BLASTP (http://blast.ncbi.nlm.nih.gov/Blast.cgi) homology searching in the genomes of MSR-1 (GenBank accession number CU459003.1), *M. magneticum* strain (GenBank accession number AP007255.1), *M. magnetotacticum* (NCBI reference sequence NZ_AAAP00000000.1), and *Magnetococcus marinus* (GenBank accession number CP000471.1), with an expectation value (E) of <1e−06 and amino acid similarity of >50%. ClustalW was used for sequence alignment. Signal sequences and peptides were predicted by using SignalP (http://www.cbs.dtu.dk/services/SignalP/) (28).

Nucleotide sequence accession number. The *nirE* sequence has been submitted to the GenBank database under accession number JN634764.

RESULTS

Identification of a *nir* cluster in MSR-1. Several *nir* genes were identified on two different contigs of the incomplete genome assembly of MSR-1. After gap closure by PCR, we found that *nirS*, encoding the nitrite reductase (cytochrome cd_1), along with all other *nir* genes (*nirTBECFDLGHJN*), is localized within a single cluster (Fig. 1A), which with some notable differences is mostly conserved in other magnetospirilla (see Fig. S1 and Table S3 in the supplemental material). *nirEFDLGHJ* are known to be necessary for d_1 heme synthesis (16–18), whereas a multiheme *c*-type cytochrome encoded by *nirT* is necessary for nitrite reduction as an endogenous electron donor in *P. stutzeri* (29), and *nirC* encodes a *c*-type cytochrome which in *P. aeruginosa* is suggested to be an electron donor for the nitrite reductase NirS (30). These genes are followed downstream by *nirN*, which encodes a *c*-type cytochrome in *Paracoccus pantotrophus*, although its function *in vivo* is not clear (31).

Deletions of *nirS* and *nirN* impair denitrification growth and magnetite synthesis. Interestingly, NirN showed conspicuous sequence similarity to NirS (43% similarity, 26% identity) (see Fig. S1C in the supplemental material), which prompted us to discern

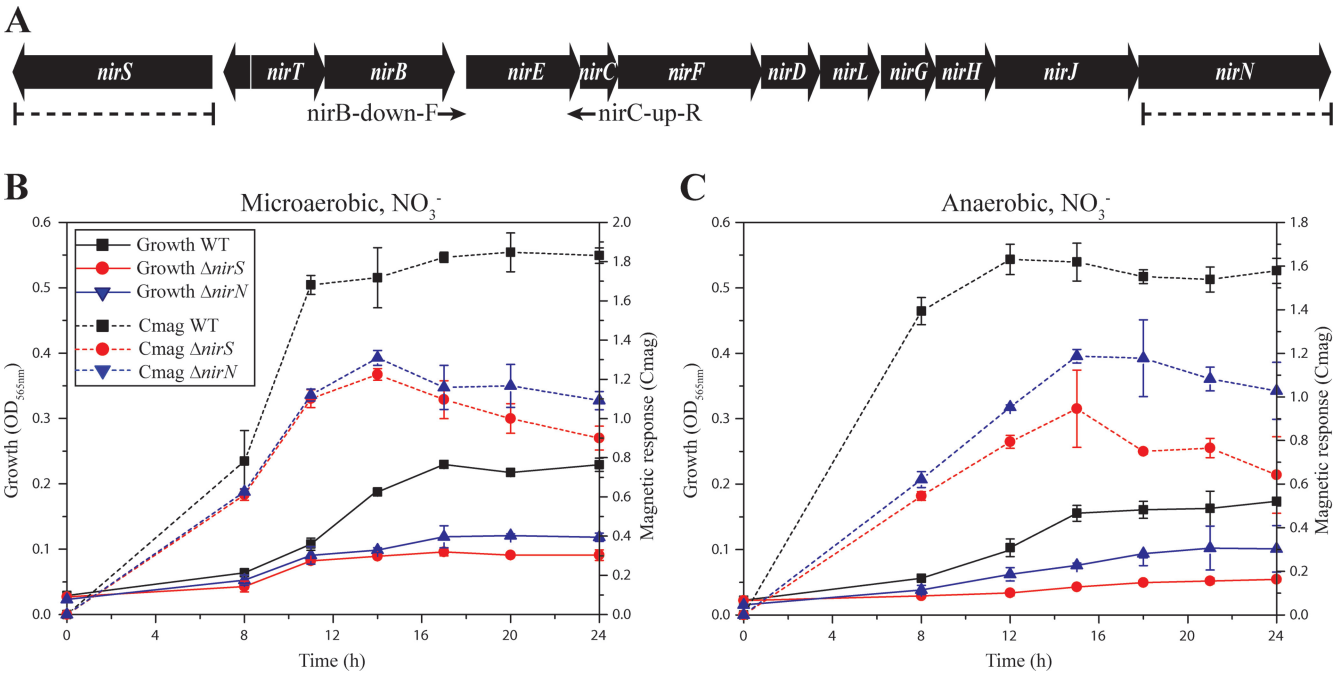

FIG 1 (A) Molecular organization of identified *nir* genes in MSR-1. Arrows indicate the PCR primers nirB-down-F and nirC-up-R, which were used for gap closure between *nirB* and *nirC* (see Materials and Methods). Dashed lines indicate the extent of deletions in Δ*nirS* and Δ*nirN* mutants. (B and C) Growth (based on the OD_{565}) and magnetic response (C_{mag}) of MSR-1 WT, Δ*nirS*, and Δ*nirN* cells under different conditions at 30°C. (B) Microaerobic, nitrate medium; (C) anaerobic, nitrate medium. Results from representative experiments were measured in triplicate, and values are given as means and standard deviations.

their individual roles in growth, magnetosome formation, and nitrite reduction by the construction of unmarked deletion mutants of both genes. The Δ*nirS* mutant displayed no difference from the WT in growth and C_{mag} under aerobic conditions in either nitrate or ammonium medium (see Fig. S2A and B). Under microaerobic conditions in ammonium medium (in the absence of nitrate), the WT and Δ*nirS* strains also reached comparable growth yields and C_{mag} values (see Fig. S2C). However, when cells were grown microaerobically in nitrate medium, both yields and C_{mag} values were significantly lower in the Δ*nirS* mutant than in the WT (Fig. 1B). Under anaerobic conditions, the Δ*nirS* mutant still grew poorly for 2 to 3 generations before growth ceased entirely. However, C_{mag} values were substantially decreased below 1.0 (Fig. 1C). TEM images revealed severe defects in magnetosome organization and crystal morphology: the anaerobic Δ*nirS* mutant produced much smaller (27.4 ± 0.7 nm, versus 49.9 ± 5.0 nm for WT crystals [means ± standard deviations]), fewer (average of 12 crystals per cell versus 35 in the WT), and irregularly shaped crystals, which were arranged in loose chains (Fig. 2A and B).

Deletion of *nirN* did not affect aerobic growth in the presence of nitrate or ammonium (see Fig. S2A and B in the supplemental material), and hardly any difference in growth or magnetite biomineralization was observed in microaerobic ammonium medium between the WT and Δ*nirN* mutant (see Fig. S2C). However, in microaerobic nitrate medium, loss of *nirN* resulted in weaker growth and lower C_{mag} values, which were only slightly higher than those in the Δ*nirS* mutant (Fig. 1B). The anaerobically grown Δ*nirN* mutant reached higher cell densities than the Δ*nirS* mutant, but the densities were still much lower than for the WT, and the C_{mag} was also much lower than in the WT, but higher than in the Δ*nirS* mutant (Fig. 1C). As shown in Fig. 2A and B, Δ*nirN* cells produced much shorter magnetosome chains (average of 7 crystals per cell, versus 35 crystals per cell in WT), whereas crystals were only slightly smaller (40.4 ± 2.0 nm, versus 49.9 ± 5.0 nm for WT). Magnetosome morphology was variable, including regular crystals in the middle of chains in addition to irregular and loosely aligned particles at the ends of chains (Fig. 2A and B). Transcomplementation of Δ*nirS* and Δ*nirN* mutants with their respective WT alleles (pLYJ51 and pLYJ74) restored denitrifying growth (data not shown) and magnetosome formation (Fig. 2C) back to the WT levels. Altogether, these results indicate that both NirS and NirN are required for WT-like denitrifying growth and magnetite biomineralization.

NirS is the only nitrite reductase, while NirN is essential for fully active nitrite reduction. Since deletion of either *nirS* or *nirN* seemed to impair denitrifying growth and magnetite biomineralization in a similar manner, we wanted to dissect their functions in nitrite reduction. First, we inoculated WT and mutant strains into deep slush agar (0.3%) tubes containing nitrate medium, in which entrapped gas bubbles are indicative for N_2 evolution. At 30°C, WT cells produced bubbles after 24 h, while in the Δ*nirS* mutant no bubbles were observed at any length of incubation, indicating a block of denitrification due to the complete absence of nitrite reduction (Fig. 3A). In contrast, Δ*nirN* cultures generated only a few bubbles after the first 24 h (data not shown) but as many as the WT after 40 h (Fig. 3A), which indicated that only NirS, and not NirN, is a genuine nitrite reductase and is sufficient for nitrite reduction in the absence of NirN.

In agreement with those results, we found WT cells growing at 30°C consumed 4 mM nitrate within 10 h, during which period only about 100 μM nitrite was transiently accumulated. However, both Δ*nirS* and Δ*nirN* cultures incubated at 30°C accumulated

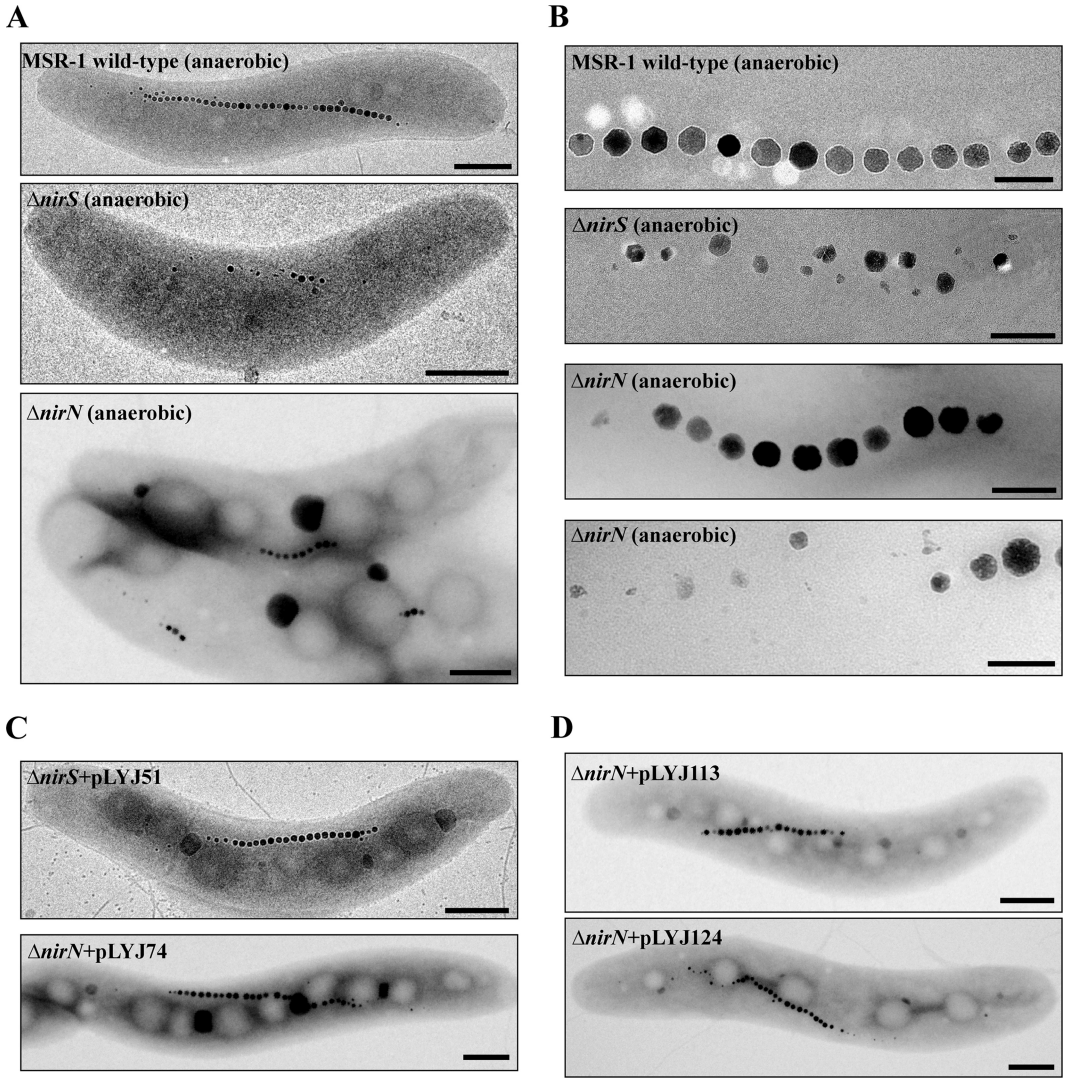

FIG 2 Effects of deletions of *nirS* and *nirN* on magnetosome formation. (A) TEM images of whole cells of (from top to bottom) WT (anaerobic, nitrate medium), Δ*nirS* mutant (anaerobic, nitrate medium), and Δ*nirN* mutant (anaerobic, nitrate medium). Bar, 500 nm. (B) Closeup views of magnetosome crystals shown in panel A. Bar, 100 nm. (C) TEM images of anaerobically grown Δ*nirS* and Δ*nirN* cells complemented with plasmids pLYJ51 and pLYJ74, respectively, harboring their WT alleles. Bars, 500 nm. (D) TEM images of anaerobically grown the Δ*nirN* strain carrying *nirN* (from top to bottom) from *M. magneticum* (*amb1408*) and *P. stutzeri* (*PST_3538*), respectively. Bar, 500 nm.

approximately 2.0 to 2.5 mM nitrite after the first 16 h in the medium, while no nitrite was detected in Δ*nirN* cultures after 48 h (data not shown). When grown at 20°C, at which temperature the WT displayed slower growth but slightly increased magnetite formation, nitrite became entirely consumed by Δ*nirN* cultures after about 7 days, again indicating that nitrite reduction still occurred in the Δ*nirN* mutant although much slower than in the WT. The roles of NirS and NirN were further assessed by following nitrate consumption and nitrite accumulation, as well as growth and magnetite formation, during anaerobic incubation at 20°C. In this experiment, nonmagnetic, aerobically grown cells were inoculated as described before (13). After a lag of 30 to 33 h, cell densities increased in WT cultures for around 15 h, after which growth ceased due to depletion of nitrate, the only added electron acceptor (Fig. 4A, panel i). During the entire growth period, C_{mag} values continuously increased, which coincided with the alignment of maturing magnetite crystals in typical chains (Fig. 4A). During the first 30 to 33 h, WT cultures consumed only a little nitrate, and then nitrate was rapidly depleted within the following approximately 30 h. Yet, nitrite accumulation was hardly detectable during the entire growth period (Fig. 4A, panel i).

Δ*nirS* cells grew slowly, to a final OD of only 0.08 after about 75 h (Fig. 4B, panel i), after which cells entirely ceased growth but continued to consume trace amounts of nitrate. Although C_{mag} values increased rapidly during the first 30 to 33 h and slightly beyond that time period, to a final value of 0.65 to 0.70, Δ*nirS* cells only produced a few irregularly shaped crystals (Fig. 4B, panels ii to v). During incubation, nitrate was gradually consumed, but approximately 0.8 to 1.0 mM remained in the culture after 90 h, while the cell densities did not increase after 75 h (Fig. 4B, panel i); the implication is that besides acting as an electron acceptor, nitrate is also assimilated and thus is a nitrogen source. Meanwhile,

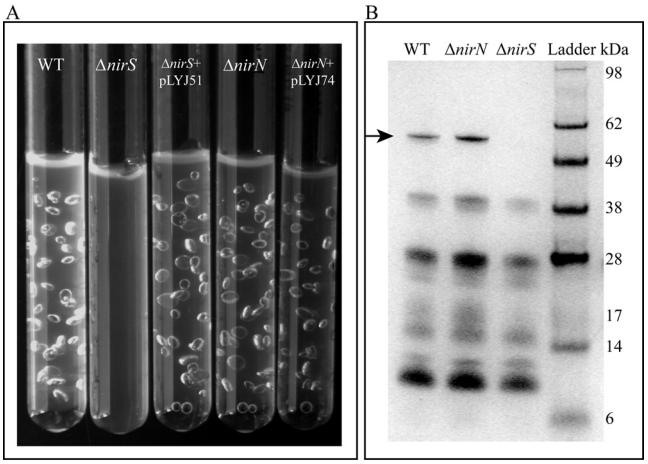

FIG 3 (A) Gas production in WT, Δ*nirS*, Δ*nirS* plus pLYJ51, Δ*nirN*, and Δ*nirN* plus pLYJ74 cultures in oxygen gradient tubes with 0.3% agar at 30°C. Δ*nirS* with pLYJ51 and Δ*nirN* with pLYJ74 cells harbored their respective WT alleles. Except for the Δ*nirN* mutant, which was incubated for 40 h, all others were cultured for 24 h. (B) Detection of heme-containing proteins. Fifty micrograms of periplasmic protein was loaded per lane. Compared to the WT and Δ*nirN* strains, the periplasmic fraction from the Δ*nirS* mutant lacked a characteristic band of cytochrome cd_1 at around 60 kDa (black arrow).

as cell densities increased slowly, nitrite gradually built up in the medium to about 2.3 to 2.5 mM after 75 h and then was not consumed further (Fig. 4B, panel i), which again demonstrated that NirS but not NirN catalyzes nitrite reduction in the absence of the other. In Δ*nirS* cultures, inorganic nitrogen (0.8 to 1.0 mM nitrate plus 2.3 to 2.5 mM nitrite) together amounted to about 3.0 to 3.5 mM at the end of growth, once again suggesting that about 0.5 to 1.0 mM nitrate was assimilated by cells from the 4 mM initially present in the medium.

When the same experiments were carried out with the Δ*nirN* mutant, during first 75 h cell densities slowly increased, as with the Δ*nirS* mutant (Fig. 4C, panel i). Then, growth transiently ceased for about 40 h, before it resumed (Fig. 4C, panel i). During first 75 h, compared to the WT, Δ*nirN* cells produced much shorter magnetosome chains with irregular and misaligned particles at chain ends resembling those shown in Fig. 2A and B (Fig. 4C, panels ii and iii), whereas during the second growth phase we frequently observed parallel chain fragments in the Δ*nirN* mutant that contained both regular and irregular magnetosome particles (Fig. 4C, TEM images b in panels iv and v) and which were never present in the Δ*nirN* mutant cultivated at 30°C. Nitrate gradually disappeared from the medium after 200 h of incubation (Fig. 4C, panel i). Coincident with this finding, nitrite transiently accumulated up to 1.8 to 2.0 mM during the first 100 h but was eventually entirely consumed as cells resumed growth (Fig. 4C, panel i). These data demonstrated that NirN *per se* is neither a nitrite reductase nor absolutely essential for nitrite reduction, but the absence of NirN lowers the activity of nitrite reduction and indirectly impairs growth and magnetite biomineralization under denitrifying conditions, in an unknown fashion.

NirN is required to synthesize the proper form of d_1 heme. Previously, NirN of *P. pantotrophus* was found to be able to bind d_1 heme *in vitro* and subsequently transfer it to the semi-*apo* cytochrome cd_1, which lacks d_1 heme, suggesting that NirN may play a role in the assembly or maturation of *holo*-NirS (31). To clarify the function of NirN in MSR-1, we analyzed the form of cytochrome cd_1 present in WT, Δ*nirS*, and Δ*nirN* cells by visible absorption spectroscopy of periplasmic extracts and by reduced alkaline pyridine ferrohemochrome analysis on the purified NirS.

NirS from MSR-1 WT displayed absorption maxima characteristic for *c* heme (409 nm for the oxidized form and 551, 522, and 418 nm for the reduced form) and d_1 heme (643 nm in the oxidized form and 663 and 620 nm in the reduced form) (Fig. 5A). However, compared to NirS homologs from nonmagnetic denitrifiers (such as *P. pantotrophus*), MSR-1 cytochrome cd_1 showed some different spectral features: the peak at 550 nm (for *c* heme) was not split, and NirS protein did not display a prominent 460-nm shoulder in the reduced form (Fig. 5A). However, this shoulder, as well as absorption peaks at 620 (attributable to d_1 heme) and 550 and 522 nm (attributable to *c* heme), were observed in a reduced alkaline pyridine ferrohemochrome spectrum of the purified cytochrome cd_1 of MSR-1 (Fig. 5B). The spectroscopic properties of *holo*-cd_1 nitrite reductase from MSR-1 were similar to those reported for the nitrite reductase from the related *M. magnetotacticum* (14). In addition, d_1 heme was also extracted from cytochrome cd_1 with acidified acetone protocol (32), with a final yield of 4.2 μM per gram (wet weight) of WT cells.

In the Δ*nirS* mutant, although we observed absorption peaks for *c* heme, neither the UV-Vis spectrum nor the reduced alkaline pyridine ferrohemochrome spectrum of periplasmic fraction showed an absorption peak for the d_1 heme (in the region of 600 to 700 nm) (Fig. 5C and D), indicating that expression of functional NirS, and thus production of NO, is required for d_1 heme biosynthesis, a conclusion which has been drawn for *P. stutzeri* and *P. pantotrophus* (33, 34). To further test whether genes for d_1 heme biogenesis are expressed in the MSR-1 Δ*nirS* mutant, we constructed a transcriptional gene fusion of *nirTBECFDLGHJN* with *gusA* (*nir-gusA*), which encoded β-glucuronidase, and transferred it into MSR-1 WT and Δ*nirS* strains by conjugation of a replicative plasmid. As shown in Table 1, WT cells containing the *nir-gusA* fusion exhibited a higher-than-3-fold level of β-glucuronidase activity under microaerobic conditions with nitrate compared to that without nitrate, whereas an increased oxygen concentration resulted in decreased β-glucuronidase activity. However, in the Δ*nirS* mutant, the expression of *nir* was neither upregulated by nitrate nor downregulated by oxygen; it only reached a similar but low level of β-glucuronidase activity (about 20 U/mg) under different tested conditions, which suggested that functional NirS protein is necessary for significant expression of *nir* genes for d_1 heme biogenesis. In addition, periplasmic fractions from the different strains (Δ*nirS*, Δ*nirN*, and WT strains) were resolved by gel electrophoresis and stained for heme-containing proteins. As expected, the WT displayed a characteristic band at around 60 kDa, which was not found in the Δ*nirS* mutant (Fig. 3B), indicating that NirS is located in the periplasm with covalently bound heme in both WT and Δ*nirN* strains, but is absent from the Δ*nirS* mutant.

In the Δ*nirN* mutant, similar to the WT, the reduced periplasmic fraction displayed absorption maxima characteristic of *c*-type cytochromes (551, 522, and 418 nm), while the oxidized form showed an absorption peak at 409 nm (Fig. 5E). However, the UV-Vis spectrum of putative d_1 heme from the periplasmic fraction was distinct from that in the WT: although the characteristic peak at 643 nm in the oxidized form for d_1 heme was present, the absorption peaks at 620 nm and 663 nm in the reduced form were missing. Instead, a new 650-nm shoulder was observed, indicating

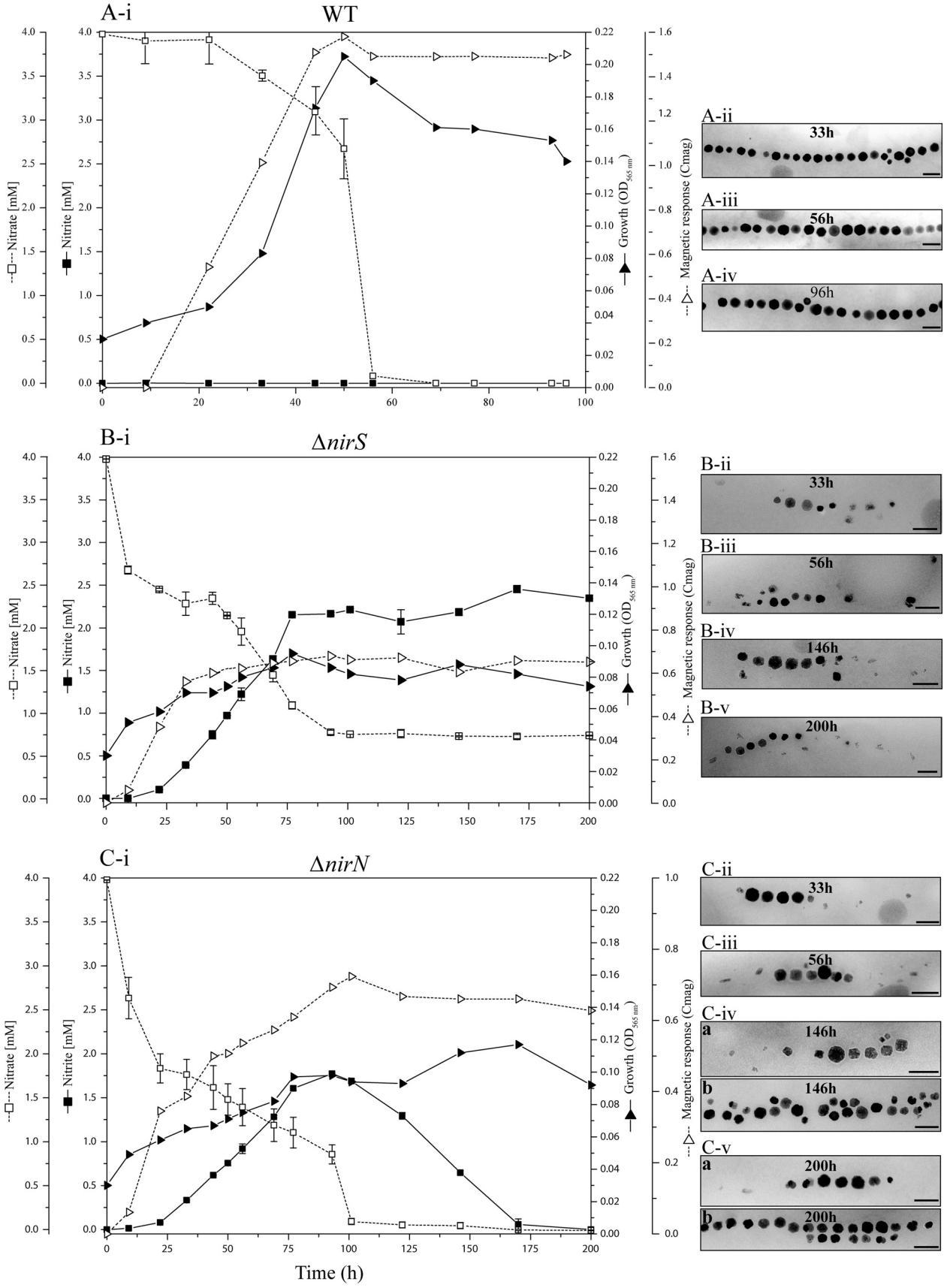

FIG 4 Left: Time courses of nitrate and nitrite utilization and magnetite biomineralization during anaerobic denitrifying growth of WT, Δ*nirS*, and Δ*nirN* strains at 20°C. The initial nitrate concentration was 4 mM, and the concentrations of nitrate and nitrite were measured over time. (Right) TEM images of WT, Δ*nirS*, and Δ*nirN* cells from aliquots taken at different time points are shown. Bars, 100 nm. The results shown come from one data set representative of two independent experiments.

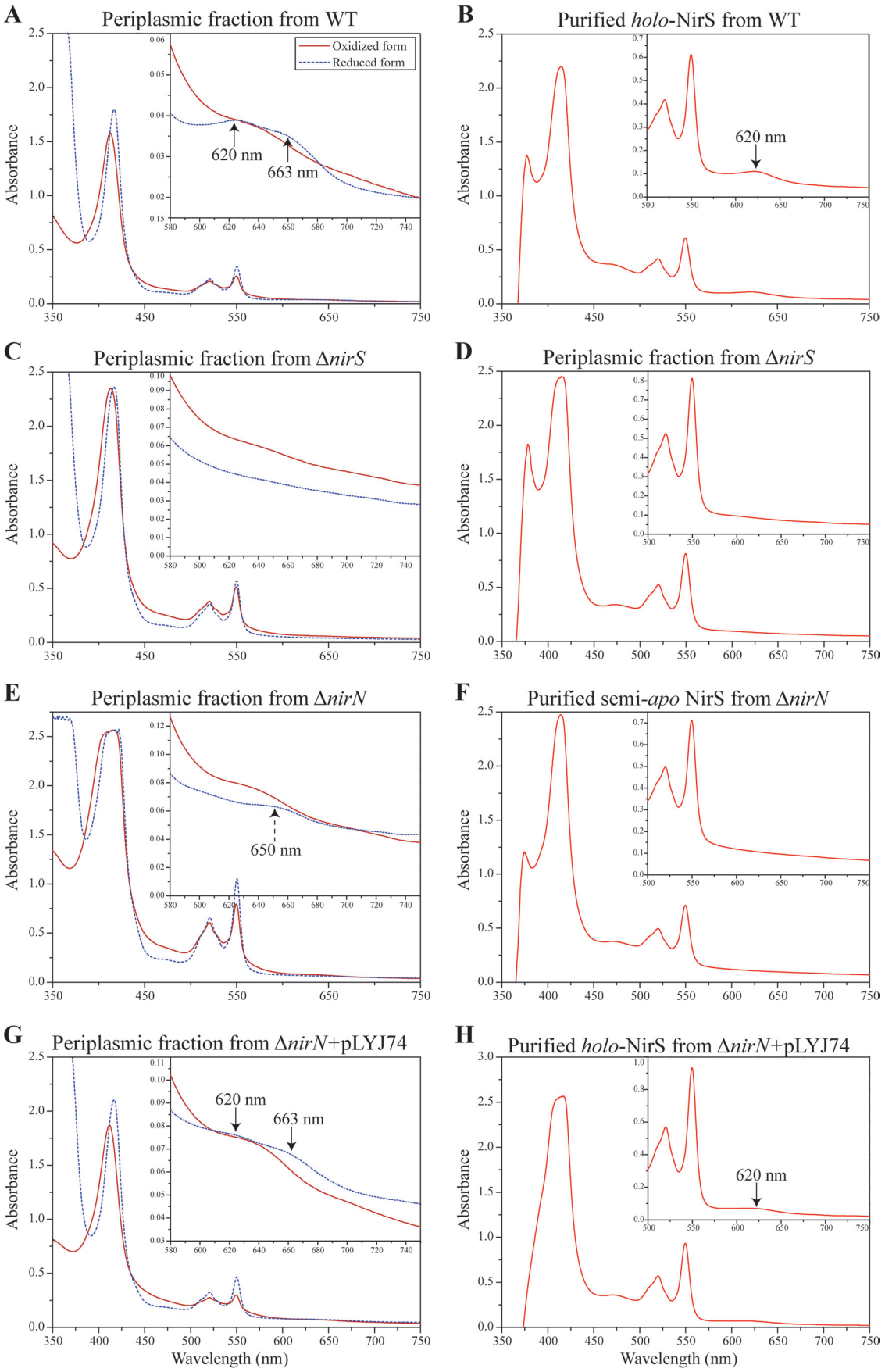
A
Periplasmic fraction from WT
Oxidized form
Reduced form
620 nm
663 nm
B
Purified holo-NirS from WT
620 nm
C
Periplasmic fraction from ΔnirS
D
Periplasmic fraction from ΔnirS
E
Periplasmic fraction from ΔnirN
650 nm
F
Purified semi-apo NirS from ΔnirN
G
Periplasmic fraction from ΔnirN+pLYJ74
620 nm
663 nm
H
Purified holo-NirS from ΔnirN+pLYJ74
620 nm
Absorbance
Wavelength (nm)

TABLE 1 Expression of transcriptional *nirTBECFDLGHJN-gusA* gene fusion in WT and Δ*nirS* strains under different conditions

Cultivation conditions	β-Glucuronidase activity (U/mg)[a]	
	WT	Δ*nirS* mutant
Microaerobic, with nitrate	99.8 ± 3.8	24.5 ± 4.5
Microaerobic, without nitrate	26.1 ± 6.9	24.2 ± 5.9
Aerobic, with nitrate	27.5 ± 3.2	21.1 ± 4.2
Aerobic, without nitrate	19.1 ± 3.4	16.4 ± 3.6

[a] The values of β-glucuronidase activity were averages of at least replicate cultures. Means and standard deviations are shown.

TABLE 2 Expression of transcriptional *nirS-gusA* gene fusion in WT and Δ*nirS* strains under anaerobic and microaerobic conditions with different nitrogen sources

Addition	β-Glucuronidase activity (U/mg)[a]			
	Anaerobic cultures		Microaerobic cultures	
	WT	Δ*nirS* mutant	WT	Δ*nirS* mutant
None[b]	ND[c]	ND	6.4 ± 1.4	10.8 ± 1.7
$NaNO_2$ (0.5 mM)	ND	ND	51.1 ± 3.3	11.9 ± 2.0
$NaNO_3$ (1 mM)	49.0 ± 4.9	16.1 ± 4.1	ND	ND
$NaNO_3$ (4 mM)	104.2 ± 14.7	25.2 ± 1.9	171.7 ± 10.3	18.6 ± 3.0
$NaNO_3$ (10 mM)	147.7 ± 25.5	20.9 ± 5.9	187.8 ± 10.4	35.2 ± 2.9

[a] Values are averages of at least replicate cultures ± standard deviations.
[b] There was no nitrate or nitrite added to the medium.
[c] ND, not determined; the β-glucuronidase activity was not measured.

that a variant form of d_1 heme was present in the Δ*nirN* mutant compared to the WT spectra (Fig. 5E). These spectral differences in WT and Δ*nirN* strains are suggestive of a different form of d_1 heme. Unexpectedly, the reduced alkaline pyridine ferrohemochrome spectrum of purified cytochrome cd_1 in the Δ*nirN* mutant lacked the characteristic d_1 heme peak at 620 nm (Fig. 5F), which suggested that no d_1 heme was present in purified NirS, or that the different form of d_1 heme might be more susceptible to dissociation from the enzyme or degradation under the aerobic conditions that were used during the purification of NirS. We also failed to detect any d_1 heme by acidified acetone extraction on the purified nitrite reductase protein from the Δ*nirN* strain, again implying that the purified nitrite reductase lacked d_1 heme. Notably, heme-stained gels of periplasmic fractions of both the control strain *P. pantotrophus* (data not shown), in which NirN is known to localize in the periplasm (31), and Δ*nirN* mutants of MSR-1 (Fig. 3B) were indistinguishable from their WT, probably due to low expression of NirN.

As shown in Fig. 5G, peaks characteristic for *c* and d_1 heme (643 and 409 nm in oxidized form and 663, 620, 551, 522, and 418 nm in reduced form) were restored in the Δ*nirN* mutant complemented with pLYJ74. Likewise, the reduced alkaline pyridine ferrohemochrome spectrum of purified cytochrome cd_1 from the Δ*nirN* mutant with pLYJ74 also displayed the WT-like shoulder at 460 nm and absorption peaks at 620, 522, and 550 nm (Fig. 5H). In agreement with this finding, we also harvested about 0.9 μM d_1 heme per gram (wet weight) from the purified cytochrome cd_1 of the Δ*nirN* complementation strain.

Because the observed phenotypic effects were different from those reported for *nirN* deletions in other, nonmagnetic denitrifiers, we wondered whether the function of NirN of MSR-1 might be somehow distinct. This idea was further supported by the presence of an additional stretch of 20 amino acids located between the d_1 heme and *c* heme binding domains that is shared by all NirN homologs from MTB but absent from their non-MTB counterparts (see Fig. S3 in the supplemental material). To test this hypothesis, we carried out transcomplementational analysis of the MSR-1 Δ*nirN* strain with *nirN* genes from *M. magneticum* and the nonmagnetic bacterium *P. stutzeri*. However, *nirN* genes from both *M. magneticum* and *P. stutzeri* were capable of fully rescuing both magnetosome formation (Fig. 2D) and nitrite reduction (data not shown) to a WT-like level without any difference, indicating that NirN homologs from magnetotactic and nonmagnetotactic bacteria have equivalent functions.

NirS is involved in nitrite-dependent iron oxidation during anaerobic biomineralization. Because all previous observations pointed toward a key role of NirS in magnetite biomineralization, we reasoned that there were two possible explanations for the observed magnetosome defects in the Δ*nirS* mutant: (i) nitrate or nitrite accumulation in Δ*nirS* mutant but not WT cultures may inhibit magnetite biomineralization via toxic effects, or (ii) the NirS protein may participate directly in magnetosome formation by oxidizing ferrous iron to produce magnetite, as hypothesized for *M. magnetotacticum* (14). To distinguish between these two possibilities, first the effects of nitrite and nitrate on *nirS-gusA* expression were investigated in WT and Δ*nirS* cultures. Expression from the *nirS* promoter increased in the WT and the Δ*nirS* mutant from 0 to 10 mM nitrate under microaerobic conditions (Table 2). Under anaerobic conditions, in the WT the same increase in expression was observed when the nitrate concentration was raised from 1 to 10 mM. However, in the Δ*nirS* mutant, 10 mM nitrate inhibited *nirS-gusA* expression. On the other hand, under microaerobic conditions, 500 μM nitrite moderately increased *nirS* expression in the WT but had no effect on *nirS* ex-

FIG 5 Spectral analysis of cytochrome cd_1 from WT, Δ*nirS* mutant, Δ*nirN* mutant, and Δ*nirN* mutant plus pLYJ74. (A) UV-visible absorption spectra of oxidized and sodium dithionite reduced periplasmic fraction from WT cells showing characteristic spectra (black arrow) for cytochrome cd_1. (B) Pyridine ferrohemochrome spectrum of purified *holo*-cytochrome cd_1 (in 50 mM Tris-HCl [pH 7.5]) from WT cells. A characteristic peak for d_1 heme at 620 nm was present (black arrow). (C) UV-visible absorption spectra of oxidized and sodium dithionite-reduced periplasmic fractions from the Δ*nirS* mutant for cytochrome cd_1. No peak for d_1 heme was found due to the deletion of *nirS*. (D) Pyridine ferrohemochrome spectrum of the periplasmic fraction (in 50 mM Tris-HCl [pH 7.5]) from the Δ*nirS* mutant. To avoid the effects from other heme-containing proteins, the periplasmic fraction was purified by DEAE chromatography before analysis. It lacked the characteristic d_1 heme absorption peak at 620 nm. (E) UV-visible absorption spectra of oxidized and sodium dithionite-reduced periplasmic fraction from the Δ*nirN* mutant for cytochrome cd_1. The absorption peaks for d_1 heme at 620 nm and 663 nm in a reduced form were missing, and instead a new 650-nm shoulder was observed (black dashed arrow). (F) Pyridine ferrohemochrome spectrum of purified semi-*apo* cytochrome cd_1 (in 50 mM Tris-HCl, pH 7.5) from the Δ*nirN* mutant. No characteristic peak for d_1 heme was found. (G) UV-visible absorption spectra of the oxidized and sodium dithionite-reduced periplasmic fractions from the Δ*nirN* mutant with pLYJ74, which carries *nirN*. The peaks characteristic for d_1 heme (643 nm in oxidized form and 663 and 620 nm in reduced form) were restored (black arrow). (H) Pyridine ferrohemochrome spectrum of purified *holo*-cytochrome cd_1 (in 50 mM Tris-HCl [pH 7.5]) from the Δ*nirN* mutant with pLYJ74 with plasmid-borne *nirN*. A characteristic peak for d_1 heme was observed (black arrow). The results shown come from one data set representative of two independent experiments.

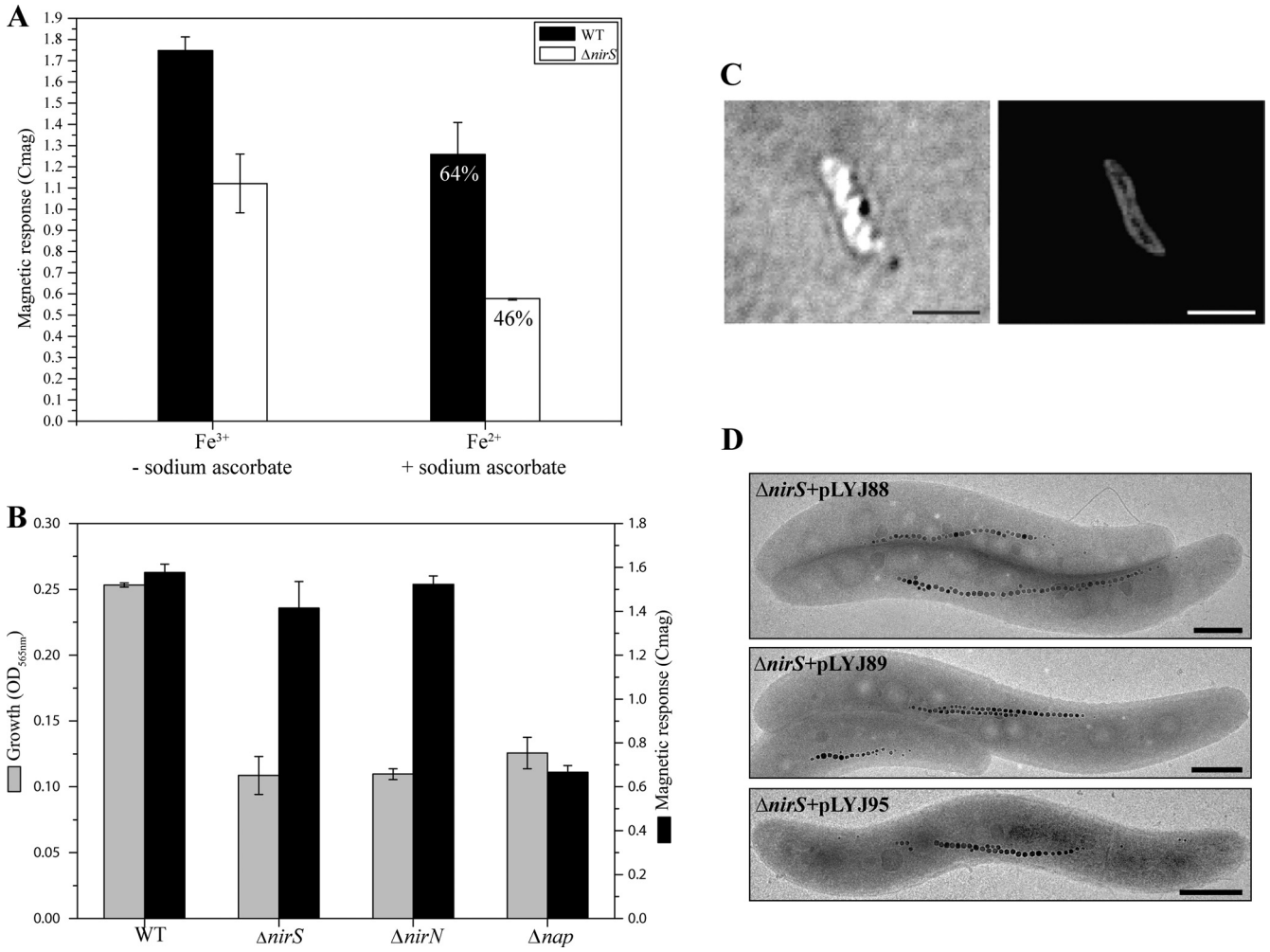

FIG 6 (A) Magnetic response (C_{mag}) of WT and Δ*nirS* mutant after three serial transfers under microaerobic conditions in iron-deprived medium. Nonmagnetic WT and the Δ*nirS* mutant were induced anaerobically for 6 h in the presence of reduced (100 μM ferrous chloride plus 0.2 mM ascorbate) and oxidized (100 μM ferric chloride) iron sources. (B) Growth (based on the OD_{565}) and magnetic response (C_{mag}) of WT, Δ*nirS*, Δ*nirN*, and Δ*nap* strains in an incubator hood with a constant atmosphere of 2% O_2 and 98% N_2. (C) Intracellular localization of the MSR-1 NirS protein N-terminally tagged with mCherry in the Δ*nirS* mutant. Differential interference contrast microscopy (left) and fluorescence microscopy (right) were used. Bar, 2 μm. (D) TEM images of the anaerobically grown Δ*nirS* mutant carrying *nirS* (top to bottom) from *M. magneticum* (*amb1395*, *amb4165*) and *P. stutzeri* (*PST_3532*), respectively. Bar, 500 nm.

pression in the Δ*nirS* mutant (Table 2). This suggests that the product of nitrite reduction, NO, rather than nitrite itself causes increased *nirS* expression, consistent with the observation that in *P. stutzeri*, *nirSTB* transcription was activated by NO but not nitrite (33). On the other hand, the Δ*nirS* mutant still showed some expression of *nirS* in the presence of nitrate, although the reaction of NO_2^- reduction to NO was blocked, indicating that NO_3^- *per se* is capable of increasing the expression of *nirS*. In line with this, the *nirS* expression level in the Δ*nap* mutant, in which denitrification is completely blocked (13), was nearly as high as that in the Δ*nirS* strain (data not shown), which further demonstrated that the product of nitrate reduction nitrite is not an inducer for *nirS* expression, whereas nitrate is able to induce the expression of *nirS*. In addition, different concentrations of nitrate and nitrite were added to microaerobically and anaerobically growing cells. Likewise, as shown for the WT before (13), neither nitrate nor nitrite had effects on growth or magnetite synthesis in the Δ*nirS* mutant (data not shown). On the other hand, the Δ*nirN* mutant also produced fewer magnetosomes, even though it consumed all transiently accumulated nitrite (Fig. 4C, TEM images in subpanels a of panels iv and v), which also demonstrated that nitrate or nitrite did not affect magnetite biomineralization.

To test whether NirS plays a role in oxidation of ferrous iron for the biomineralization of the mixed-valence oxide magnetite [$FeII(FeIII)_2O_4$], growth experiments in the presence of fully reduced (100 μM ferrous chloride plus 0.2 mM ascorbate) and fully oxidized (100 μM ferric chloride) iron sources were performed under anaerobic conditions. Iron-deprived nonmagnetic cells were inoculated to a final OD_{565} of 0.1. More than 6 h after inoculation, if only ferrous iron was available, the C_{mag} of the WT was about 64% of that in the presence of ferric iron (Fig. 6A). A decrease was also observed for the Δ*nirS* mutant; however, the difference in the C_{mag} between reducing and oxidizing conditions was markedly larger (about 46% of that under oxidizing conditions) than in the WT. Consistent with previous reports that ferrous iron can be chemically oxidized

by nitrite or nitrous oxide (35), the ferrozine assay showed that ferrous iron was completely oxidized to ferric iron in the Δ*nirS* culture by the accumulated nitrite. In contrast, in the WT no detectable oxidation of ferrous iron was found, as in the noninoculated control, implying that in the Δ*nirS* mutant ferrous iron becomes oxidized anaerobically by accumulated nitrite. Thus, the reduced C_{mag} of the Δ*nirS* mutant in ferrous iron medium may result from the combined effects of only ferrous iron being present initially and its subsequent rapid and complete oxidation to ferric iron. Therefore, to maintain a permanent supply of ferrous iron and to prevent complete chemical oxidation of all ferrous iron by nitrite in the Δ*nirS* mutant, washed nonmagnetic cells were suspended in nitrate-free LIM to a final OD_{565} of 0.1 and incubated under anaerobic conditions in the presence of either ferrous or ferric iron. However, no magnetic response was found in either MSR-1 WT or Δ*nirS* mutant cultures after incubation for 6 h (data not shown). This demonstrated that the presence of nitrate is essential for supplying energy for growth and magnetite biomineralization under strictly anaerobic conditions. Furthermore, when the Δ*nirS* or Δ*nirN* mutant was incubated at a constant oxygen concentration of 2% in the presence of nitrate, for both of them magnetosome formation was rescued to the WT level, indicating that in the absence of nitrite reduction, ferrous iron is oxidized by oxygen to ferric iron (Fig. 6B). However, in the Δ*nap* mutant, in which microaerobic magnetite biosynthesis is also impaired in the absence of nitrate (13), no obvious difference was detected between oxygen-limited cultures (grown in 20-ml sealed Hungate tubes with 10 ml of medium under 2% O_2) and those exposed to the same oxygen concentration in the nonlimiting atmosphere of an incubator hood (Fig. 6B). This again indicated that NirS is capable of oxidizing ferrous to ferric iron for anaerobic magnetosome formation during reduction of nitrite to nitric oxide, and the decreased C_{mag} under sealed microaerobic conditions was caused by oxidant limitation.

It was suggested previously that iron oxidation activity might be a specific property of NirS proteins from MTB species, as only NirS from *M. magnetotacticum* showed Fe(II):nitrite oxidoreductase activity *in vitro*, whereas NirS from *P. aeruginosa* lacked this activity (14). On the other hand, most of NirS of *M. magnetotacticum* was detected in the periplasmic fraction, and a putative spatial connection with the magnetosome membrane was inferred (14). As predicted by using the SignalP program (28), our functional MSR-1 NirS-mCherry fusion (as shown by its ability to complement the Δ*nirS* mutant) displayed an evenly distributed periplasmic fluorescence in the Δ*nirS* mutant, much like that reported for NirS proteins from nonmagnetic denitrifying bacteria (Fig. 6C), but it lacked the characteristic filamentous signal of magnetosome proteins (26, 36), indicating that magnetosomal localization is not required for its function in biomineralization. As shown in Fig. 6D, all tested plasmids carrying different *nirS* genes from either the magnetic *M. magneticum* (*amb1395* and *amb4165*) or the nonmagnetic bacterium *P. stutzeri* (*PST_3532*) rescued both growth and magnetite synthesis in the Δ*nirS* mutant to levels comparable to the WT. These data indicate that nitrite reductases of magnetic and nonmagnetic denitrifying bacteria are functionally equivalent with respect to both denitrification and magnetite biomineralization.

DISCUSSION

The conspicuous sequence similarity to NirS of NirN suggested a similar or related function and raised the question of whether NirN itself may catalyze nitrite reduction. However, despite the superficially similar phenotypes in denitrifying growth and biomineralization, closer inspection revealed that, whereas deletion of *nirS* abolished nitrite reduction completely, the Δ*nirN* mutant was still capable of nitrite reduction upon prolonged incubation at different temperatures (20°C or 30°C), although utilization of nitrate and nitrite was substantially attenuated compared to WT. This demonstrated that NirN alone is not able to support nitrite reduction in the absence of NirS, and NirN plays an indirect role in nitrite reduction. Based on *in vitro* data for NirN from *P. pantotrophus*, NirN was suggested to possibly function as a d_1 donor in the assembly of d_1 heme into NirS (31). Our biochemical and *in vivo* data are consistent with this assumption, because the form of periplasmic d_1 heme from the Δ*nirN* mutant was different from the WT. Likewise, cytochrome cd_1 (NirS) purified from the Δ*nirN* mutant only displayed absorption maxima of *c*-type but no d_1-type heme, possibly due to an aberrant form of d_1 heme. Thus, besides maintaining a correct form of d_1 heme, NirN might be further required for capture and subsequent transfer of a functional d_1 heme to semi-*apo* NirS, as speculated before (31). As a consequence, in the Δ*nirN* strain, d_1 heme cannot be properly assembled in NirS, resulting in poor nitrite-reducing activity. This different form of d_1 heme from the Δ*nirN* strain might be more sensitive to oxygen and therefore be degraded under our conditions of preparation. Intriguingly, the effect of *nirN* deletion on magnetite biomineralization was partly compensated by growing the cells at 20°C. The lower temperature is favorable for magnetite biomineralization in the WT, although it causes slower growth, which might facilitate the assembly of heme d_1 into NirS in the absence of NirN. Alternatively, NirN might ensure the proper assembly of heme d_1 at elevated temperatures by a chaperone-like function, required in particular under growth conditions atypical for a moderately psychrophilic bacterium from a freshwater environment. However, the suggested NirN function does not seem to be a peculiarity of MSR-1, since in our cross-complementation experiments, all tested *nirN* homologs from various magnetic and nonmagnetic denitrifiers restored denitrifying growth, nitrite reduction, and magnetosome formation of the Δ*nirN* mutant back to WT-like levels. Although NirN proteins are conserved in all bacterial *nir* clusters, their physiological function is unknown, as no phenotypic effects could be assigned to any *nirN* deletion in various analyzed denitrifiers (16, 30, 31). Thus, our study provides the first evidence for a physiological function of NirN *in vivo*. The different phenotypes in MSR-1 and nonmagnetic denitrifiers may be also explained by the unusually high susceptibility of MSR-1 to nitrate (<20 mM) and nitrite (<1.5 mM) (13), while nonmagnetic nitrate reducers are capable of growth in the presence of much higher concentrations (16, 31), making MSR-1 less tolerant to any impairment in the detoxifying reduction of nitrite.

While NirN is likely linked to biomineralization only indirectly through a functional interaction with NirS, our data argue for a more direct role of the nitrite reductase NirS. In contrast to Nap, NirS is not absolutely required for anaerobic respiration, which substantiates the previous finding that nitrate reduction catalyzed by Nap is the primary energy-generating process in denitrification of MSR-1 (13). In *M. magneticum*, a similar phenotype (poor an-

aerobic growth, impaired magnetite synthesis) was observed upon concomitant interruption of *norB* and *nirS* (*amb1395*) (37). Since an additional *nirS* homolog (*amb4165*) is present in the *M. magneticum* genome, the results of Wang et al. (37) imply that Amb1395 might be the main nitrite reductase, while Amb4165 has no significant function in denitrification and magnetite synthesis. However, in our experiments, both *amb1395* and *amb4165* from *M. magneticum* when placed under the control of the *nirS* promoter region from MSR-1 were able to fully restore WT-like growth and magnetosome formation in the MSR-1 Δ*nirS* mutant, indicating that the speculated lack of *amb4165* function might be due to transcriptional inactivity under the test conditions.

Taken together, the observed defects in magnetite biomineralization in the Δ*nirS* mutant are not directly caused by the accumulation of nitrite, as we concluded from the following observations: (i) although nitrite accumulated up to 1 to 2 mM when cells of the WT (13) and Δ*nirS* mutant were incubated under a constant microaerobic atmosphere, no effect was found on magnetite biomineralization; (ii) as shown for the WT before (13), concentrations of added nitrate (20 mM) and nitrite (2.5 mM) had no effect on biomineralization in the Δ*nirS* mutant (data not shown); (iii) a Δ*nirN* culture still displayed defects in magnetite biomineralization, even though all nitrite was depleted from the medium at the end of incubation. Another possible explanation for impaired biomineralization in the Δ*nirS* mutant might be the energy limitation in poorly growing cells. However, we never observed similar severe defects in magnetite synthesis upon deletions of other terminal oxidases, such as cbb_3, for aerobic respiration, which also caused very poor growth but had no obvious effect on magnetosome morphology under microaerobic conditions in the absence of nitrate (Y. Li and D. Schüler, unpublished data). Taken together, these data suggest that the observed effects on magnetite biosynthesis in the Δ*nirS* mutant are directly associated with its enzymatic activity, which is consistent with the proposed Fe(II):nitrite oxidoreductase function of NirS in magnetospirilla (14) and might be explained by an unbalanced ferrous-to-ferric iron ratio required for the formation of the mixed-valence iron oxide magnetite [$FeII(FeIII)_2O_4$] in the Δ*nirS* mutant when ferrous iron oxidation is limited (i.e., in the absence of oxygen). In contrast to earlier speculations that iron-oxidizing activity is a function specific to nitrite reductases of MTB (14), we demonstrated that the suspected iron-oxidizing activity is not confined to NirS of magnetospirilla but might be a property common to other cytochrome cd_1 nitrite reductases. Taken together, these findings suggest that the impaired magnetite synthesis in the Δ*nirS* mutant is likely a consequence of decreased oxidation of ferrous iron, which in the WT takes places in the periplasm with nitrite as electron acceptor catalyzed by NirS. On the other hand, ferrous iron can also be chemically oxidized with nitrite (35, 38), and nitrite and oxygen are potent oxidants for ferrous iron also in ferrite plating, a chemical method for the preparation of magnetite films (39). Therefore, magnetite biomineralization might be favored by combined abiogenic oxidation and bioenzymatic catalysis.

In conclusion, our genetic and biochemical analyses revealed that the reduction of nitrite to nitric oxide requires the activity of NirS and that proper assembly of d_1 heme in *holo*-NirS depends on the functional interaction with NirN, a protein with previously unknown function. Although in some other magnetosome-biomineralizing bacteria, such as *Magnetococcus marinus*, *nir* genes are absent, consistent with the reported inability to grow by denitrification (40, 41), our data demonstrated that enzymatic nitrite reduction, besides its key respiratory function, also participates in redox homeostasis required for magnetite biomineralization under oxidant-limited conditions (i.e., anaerobic growth) in magnetospirilla. This presents further evidence that, in addition to specific and essential functions provided by proteins encoded within the genomic magnetosome island, the biosynthesis of magnetosomes also relies on a number of auxiliary functions contributed by general metabolism.

ACKNOWLEDGMENTS

We thank Heinrich Jung, Ludwig-Maximilians-Universität München, for strain *P. stutzeri*.

The China Scholarship Council is greatly acknowledged for financial support (Y. Li).

REFERENCES

1. **Jogler C, Schüler D.** 2009. Genomics, genetics, and cell biology of magnetosome formation. Annu. Rev. Microbiol. **63:**501–521.
2. **Ullrich S, Kube M, Schübbe S, Reinhardt R, Schüler D.** 2005. A hypervariable 130-kilobase genomic region of *Magnetospirillum gryphiswaldense* comprises a magnetosome island which undergoes frequent rearrangements during stationary growth. J. Bacteriol. **187:**7176–7184.
3. **Murat D, Quinlan A, Vali H, Komeili A.** 2010. Comprehensive genetic dissection of the magnetosome gene island reveals the step-wise assembly of a prokaryotic organelle. Proc. Natl. Acad. Sci. U. S. A. **107:**5593–5598.
4. **Lohsse A, Ullrich S, Katzmann E, Borg S, Wanner G, Richter M, Voigt B, Schweder T, Schüler D.** 2011. Functional analysis of the magnetosome island in *Magnetospirillum gryphiswaldense*: the *mamAB* operon is sufficient for magnetite biomineralization. PLoS One **6**(10):e25561. doi:10.1371/journal.pone.0025561.
5. **Mann S, Sparks NHC, Board RG.** 1990. Magnetotactic bacteria: microbiology, biomineralization, palaeomagnetism and biotechnology. Adv. Microb. Physiol. **31:**125–181.
6. **Faivre D, Agrinier P, Menguy N, Zuddas P, Pachana K, Gloter A, Laval J, Guyot F.** 2004. Mineralogical and isotopic properties of inorganic nanocrystalline magnetites. Geochim. Cosmochim. Acta **68:**4395–4403.
7. **Faivre D, Böttger LH, Matzanke BF, Schüler D.** 2007. Intracellular magnetite biomineralization in bacteria proceeds by a distinct pathway involving membrane-bound ferritin and an iron(II) species. Angew. Chem. Int. Ed. Engl. **46:**8495–8499.
8. **Yang CD, Takeyama H, Tanaka T, Matsunaga T.** 2001. Effects of growth medium composition, iron sources and atmospheric oxygen concentrations on production of luciferase-bacterial magnetic particle complex by a recombinant *Magnetospirillum magneticum* AMB-1. Enzyme Microb. Technol. **29:**13–19.
9. **Heyen U, Schüler D.** 2003. Growth and magnetosome formation by microaerophilic *Magnetospirillum* strains in an oxygen-controlled fermentor. Appl. Microbiol. Biotechnol. **61:**536–544.
10. **Blakemore RP, Short KA, Bazylinski D, Rosenblatt C, Frankel R.** 1985. Microaerobic conditions are required for magnetite formation within *Aquaspirillum magnetotacticum*. Geomicrobiol. J. **4:**53–71.
11. **Bazylinski D, Blakemore RP.** 1983. Denitrification and assimilatory nitrate reduction in *Aquaspirillum magnetotacticum*. Appl. Environ. Microbiol. **46:**1118–1124.
12. **Zumft WG.** 1997. Cell biology and molecular basis of denitrification. Microbiol. Mol. Biol. Rev. **61:**533–616.
13. **Li Y, Katzmann E, Borg S, Schüler D.** 2012. The periplasmic nitrate reductase Nap is required for anaerobic growth and involved in redox control of magnetite biomineralization in *Magnetospirillum gryphiswaldense*. J. Bacteriol. **194:**4847–4856.
14. **Yamazaki T, Oyanagi H, Fujiwara T, Fukumori Y.** 1995. Nitrite reductase from the magnetotactic bacterium *Magnetospirillum magnetotacticum*: a novel cytochrome cd_1 with Fe(II)-nitrite oxidoreductase activity. Eur. J. Biochem. **233:**665–671.
15. **Rinaldo S, Sam KA, Castiglione N, Stelitano V, Arcovito A, Brunori M, Allen JWA, Ferguson SJ, Cutruzzolà F.** 2011. Observation of fast release of NO from ferrous d_1 haem allows formulation of a unified reaction mechanism for cytochrome cd_1 nitrite reductases. Biochem. J. **435:**217–225.

16. **Kawasaki S, Arai H, Kodama T, Igarashi Y.** 1997. Gene cluster for dissimilatory nitrite reductase (*nir*) from *Pseudomonas aeruginosa*: sequencing and identification of a locus for heme d_1 biosynthesis. J. Bacteriol. **179:**235–242.
17. **Bali S, Lawrence AD, Lobo SA, Saraiva LM, Golding BT, Palmer DJ, Howard MJ, Ferguson SJ, Warren MJ.** 2011. Molecular hijacking of siroheme for the synthesis of heme and d_1 heme. Proc. Natl. Acad. Sci. U. S. A. **108:**18260–18265.
18. **Palmedo G, Seither P, Korner H, Matthews JC, Burkhalter RS, Timkovich R, Zumft WG.** 1995. Resolution of the *nirD* locus for heme d_1 synthesis of cytochrome cd_1 (respiratory nitrite reductase) from *Pseudomonas stutzeri*. Eur. J. Biochem. **232:**737–746.
19. **Faivre D, Menguy N, Posfai M, Schüler D.** 2008. Environmental parameters affect the physical properties of fast-growing magnetosomes. Am. Mineral. **93:**463–469.
20. **Schüler D, Uhl R, Bäuerlein E.** 1995. A simple light scattering method to assay magnetism in *Magnetospirillum gryphiswaldense*. FEMS Microbiol. Lett. **132:**139–145.
21. **Schüler D, Baeuerlein E.** 1998. Dynamics of iron uptake and Fe_3O_4 biomineralization during aerobic and microaerobic growth of *Magnetospirillum gryphiswaldense*. J. Bacteriol. **180:**159–162.
22. **Sambrook J, Russel D.** 2001. Molecular cloning: a laboratory manual, 3rd ed. Cold Spring Harbor Laboratory Press, Cold Spring Harbor, NY.
23. **Goodhew CF, Brown KR, Pettigrew GW.** 1986. Heme staining in gels, a useful tool in the study of bacterial *c*-type cytochromes. Biochim. Biophys. Acta **852:**288–294.
24. **Bartsch RG, Kakuno T, Horio T, Kamen MD.** 1971. Preparation and properties of *Rhodospirillum rubrum* cytochromes c_2, cc′, and $b_{557.5}$, and flavin mononucleotide protein. J. Biol. Chem. **246:**4489–4496.
25. **Viollier E, Inglett PW, Hunter K, Roychoudhury AN, Van Cappellen P.** 2000. The ferrozine method revisited: Fe(II)/Fe(III) determination in natural waters. Appl. Geochem. **15:**785–790.
26. **Katzmann E, Scheffel A, Gruska M, Plitzko JM, Schüler D.** 2010. Loss of the actin-like protein MamK has pleiotropic effects on magnetosome formation and chain assembly in *Magnetospirillum gryphiswaldense*. Mol. Microbiol. **77:**208–224.
27. **Katzmann E, Müller FD, Lang C, Messerer M, Winklhofer M, Plitzko JM, Schüler D.** 2011. Magnetosome chains are recruited to cellular division sites and split by asymmetric septation. Mol. Microbiol. **82:**1316–1329.
28. **Petersen TN, Brunak S, von Heijne G, Nielsen H.** 2011. SignalP 4.0: discriminating signal peptides from transmembrane regions. Nat. Methods **8:**785–786.
29. **Jüngst A, Wakabayashi Matsubara S, Zumft H, WG.** 1991. The *nirSTBM* region coding for cytochrome cd_1-dependent nitrite respiration of *Pseudomonas stutzeri* consists of a cluster of mono-, di-, and tetraheme proteins. FEBS Lett. **279:**205–209.
30. **Hasegawa N, Arai H, Igarashi Y.** 2001. Two *c*-type cytochromes, NirM and NirC, encoded in the *nir* gene cluster of *Pseudomonas aeruginosa* act as electron donors for nitrite reductase. Biochem. Biophys. Res. Commun. **288:**1223–1230.
31. **Zajicek RS, Bali S, Arnold S, Brindley AA, Warren MJ, Ferguson SJ.** 2009. d_1 haem biogenesis: assessing the roles of three *nir* gene products. FEBS J. **276:**6399–6411.
32. **Hill KE, Wharton DC.** 1978. Reconstitution of apoenzyme of cytochrome oxidase from *Pseudomonas aeruginosa* with heme d_1 and other heme groups. J. Biol. Chem. **253:**489–495.
33. **Vollack KU, Zumft WG.** 2001. Nitric oxide signaling and transcriptional control of denitrification genes in *Pseudomonas stutzeri*. J. Bacteriol. **183:**2516–2526.
34. **Zajicek RS, Cartron ML, Ferguson SJ.** 2006. Probing the unusual oxidation/reduction behavior of *Paracoccus pantotrophus* cytochrome cd_1 nitrite reductase by replacing a switchable methionine heme iron ligand with histidine. Biochemistry **45:**11208–11216.
35. **Moraghan JT, Buresh RJ.** 1977. Chemical reduction of nitrite and nitrous oxide by ferrous iron. Soil Sci. Soc. Am. J. **41:**47–50.
36. **Lang C, Schüler D.** 2008. Expression of green fluorescent protein fused to magnetosome proteins in microaerophilic magnetotactic bacteria. Appl. Environ. Microbiol. **74:**4944–4953.
37. **Wang K, Ge X, Bo T, Chen Q, Chen G, Liu W.** 2011. Interruption of the denitrification pathway influences cell growth and magnetosome formation in *Magnetospirillum magneticum* AMB-1. Lett. Appl. Microbiol. **53:**55–62.
38. **Vancleemput O, Baert L.** 1983. Nitrite stability influenced by iron compounds. Soil Biol. Biochem. **15:**137–140.
39. **Abe M.** 2000. Ferrite plating: a chemical method preparing oxide magnetic films at 24–100 degrees C, and its applications. Electrochim. Acta **45:**3337–3343.
40. **Frankel RB, Bazylinski DA, Johnson MS, Taylor BL.** 1997. Magneto-aerotaxis in marine coccoid bacteria. Biophys. J. **73:**994–1000.
41. **Schübbe S, Williams T, Xie G, Kiss H, Brettin T, Martinez D, Ross C, Schüler D, Cox B, Nealson K, Bazylinski D.** 2009. Complete genome sequence of the chemolithoautotrophic marine *magnetotactic coccus* strain MC-1. Appl. Environ. Microbiol. **75:**4835–4852.